ACS APPLIED POLYMER MATERIALS

pubs.acs.org/acsapm

Article

High-Pressure Synthesis of Highly Conjugated Polymers via Synergistic Polymerization of Phenylpropiolic Acid

Xuan Wang, Xingyu Tang, Xin yang, Yida Wang, Peijie Zhang, Xiao Dong, Dongliang Yang, Xujie Lü, Haiyan Zheng, Kuo Li,* and Ho-kwang Mao

HPSTAR 1503-2022

Cite This: *ACS Appl. Polym. Mater.* 2022, 4, 5246−5252

Read Online

ACCESS | Metrics & More | Article Recommendations | Supporting Information

ABSTRACT: The synergistic reaction between alkyne and phenyl groups is a promising pathway for decreasing the reaction pressures of aromatics and enabling scalable high-pressure synthesis of carbon materials via pressure-induced polymerization (PIP). Here by combining theoretical calculations and experimental data, we demonstrate that a simultaneous polymerization of alkynyl and phenyl groups occurred in phenylpropiolic acid (PPA) with the threshold distance $d_{C\cdots C}$ = 3.3 Å, generating an extended structure consisting of sp^2 and sp^3 carbons. The reaction pressure of phenyl was significantly decreased to ∼5 GPa, which can be applied for large-scale synthesis. The product has a large π-electron conjugated system, resulting in a band gap energy reduced to 1.65 eV and an electrical conductivity increasing to 1.24×10^{-6} S · cm^{-1}. Our research confirmed that conjugated polymers can be synthesized at lower pressures via the high-pressure synergistic reaction route of phenylethynyl compounds and can be used to further realize applications in organic photovoltaic devices.

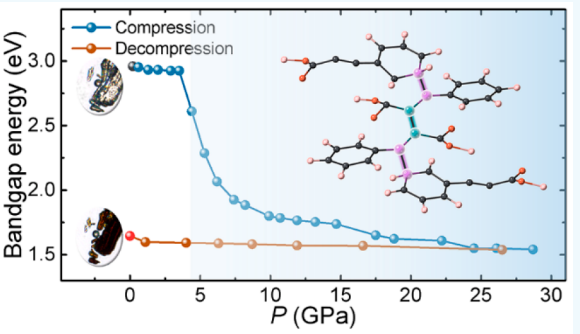

KEYWORDS: *pressure-induced polymerization, phenylpropiolic acid, conjugated polymer, synergistic polymerization, phenylethynyl compounds*

INTRODUCTION

Pressure-induced polymerization (PIP) is one of the most promising synthetic approaches for constructing carbon materials. This solid-state polymerization method tends to follow topochemical reaction routes for the precise synthesis of new carbon-based materials with more saturated and dense structures.[1−4] The unsaturated groups like alkenyl,[5,6] alkynyl,[7−11] and aromatic rings[12−18] can be activated without catalyst and irreversibly bonded to form high-density carbon materials with covalent-bond chains or networks. For example, 1D polyacetylene, carbon nanothreads, N-doped nanothreads, 2D F-doped graphene have been synthesized by compressing acetylene,[8] benzene,[12] pyridine,[15] aniline,[16] 1,2-diazine,[17] and benzene-hexafluorobenzene cocrystal.[19] Compared to the aromatics, alkynes tend to have higher reactivity and lower reaction pressure thresholds at ambient temperature. In the study of 1,3,5-triethynylbenzene (TEB)[20] and 1,4-diphenylbutadiyne (DPB),[21] phenyl reacts with phenylethynyl via a [4 + 2] dehydro-Diels−Alder (DDA) reaction driven by crystal alignment, and produces crystalline graphitic nanoribbons at pressures far below 20 GPa. This is different from the reaction of the C≡C bonds alone in the polymerization reaction of phenylacetylene,[11] suggesting the introduction of alkynyl induces the synergetic reaction with phenyl groups. The reaction path was significantly affected, and the pressure of PIP was effectively reduced. The product conjugated polymer with a low optical bandgap, increases the absorption in visible and near-infrared bands. It has potential applications in the field of high-efficiency organic photovoltaic devices.

Different from the high reaction activity of these groups, amino and carboxyl groups usually exhibit high structural stability under high pressure because of the intermolecular hydrogen bonds, which are used to maintain the ordered arrangement and obtain crystalline polymeric products. By introducing NH_2 groups into benzene, aniline is polymerized under high pressure to obtain crystalline products assisted by H-bonds.[16] The orderly arrangement of acetylenedicarboxylic acid restrained by the intermolecular hydrogen bonds between the carboxyl groups results in the topochemical polymerization of C≡C bonds and the formation of poly dicarboxylacetylene.[22] On the basis of the present experience, we propose that carboxyl groups would help phenylacetylenes to stabilize the ordered molecular stacking in polymerization. Thus, in this

Received: May 4, 2022
Accepted: June 16, 2022
Published: June 28, 2022

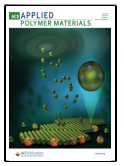

ACS Publications

© 2022 American Chemical Society

https://doi.org/10.1021/acsapm.2c00728
ACS Appl. Polym. Mater. 2022, 4, 5246−5252

work, we investigated PIP of phenylpropiolic acid (PPA) (see Scheme 1). A synergistic polymerization of alkynyl-phenyl group at 5 GPa was demonstrated by in situ Raman and infrared (IR) spectroscopy, during which the hydrogen bond preserved an ordered arrangement of the molecules. Combined with metadynamic (MD) simulation, it was proved that the product structure contains a large π-electron conjugation system, which corresponds to the bandgap changes observed in the UV−vis absorption spectra.

Scheme 1. Chemical Structure of Phenylpropiolic Acid

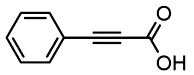

EXPERIMENTAL SECTION

In Situ High-Pressure Experiments of PPA. PPA (purity ≥ 98%) was purchased from MERYER (Shanghai), and used without further purification. For the in situ high-pressure Raman, IR absorption, UV−vis absorption, and powder X-ray diffraction (XRD) experiments, PPA was loaded in to a symmetric diamond anvil cell (DAC) with an anvil culet diameter of d_{culet} = 300 μm. Type II-a diamonds were used for IR and UV−vis experiments to avoid absorption band at 1000−1300 cm^{-1}. Gaskets (T301 stainless steel) were preindented to a thickness of ∼35 μm, and a center hole with d = 150 μm was drilled as the sample chamber. The pressure was calibrated according to the ruby fluorescence equation[23]

$$P(\mathrm{GPa}) = 248.4[(\lambda/\lambda_0)^{7.665} - 1] \quad (1)$$

Where λ_0 (694.25 nm) and λ are the wavelengths of the R1 ruby fluorescence line at ambient pressure and current pressure.

Raman experiments were carried out on a Renishaw Micro-Raman spectroscopy system equipped with a 532 nm Nd:YAG laser (2400 lines/mm grating). The system was calibrated by the Raman signal of Si. The continuous mode was chosen and the exposure intensity was 10%, with exposure time of 20 s per point.

The sample for IR experiment was prepared as described previously,[22] and a KBr slice was used for PPA sample thinning. The conventional source was Globar. The Mid-IR spectra were collected in transmission mode in the range of 600−4000 cm^{-1} on a Bruker VERTEX 70v with HYPERION 2000 microscope. The resolution was 2 cm^{-1} through a 20 × 20 μm^2 aperture. The IR absorption spectrum of DAC filled with KBr in the same aperture region was used as the background.

In situ high-pressure powder XRD data were collected at 4W2 beamline at the Beijing Synchrotron Radiation Facility (BSRF). The incident X-ray was monochromatized to a wavelength of 0.6199 Å. A Pilatus 2M detector at 4W2 was used and the geometry was calibrated by CeO_2. The collected 2D XRD patterns were integrated by the *Dioptas* program.[24] Lebail fitting and Rietveld refinement were performed using *Jana2006* software.[25]

The single crystal of PPA was prepared by slowly evaporating its ethanol solution. The PPA crystals were loaded inside the sample chamber; silicone oil was used as the pressure transmitting medium, and its absorption was used for background calibration in UV−vis experiments. The absorption spectra and optical micrographs were measured in a home-designed spectroscopy system (Gora-UVN-FL, assembled by Ideaoptics, Shanghai, China). UV−vis absorption spectra were collected using a xenon light source with wavelength range of 320−850 nm. The bandgap measured by absorption method is determined by extrapolating the linear portion of the $\alpha^{1/2}$ versus of the $h\nu$ curve, where α is the absorption coefficient, h is the Planck constant, and ν is the frequency of the photon.

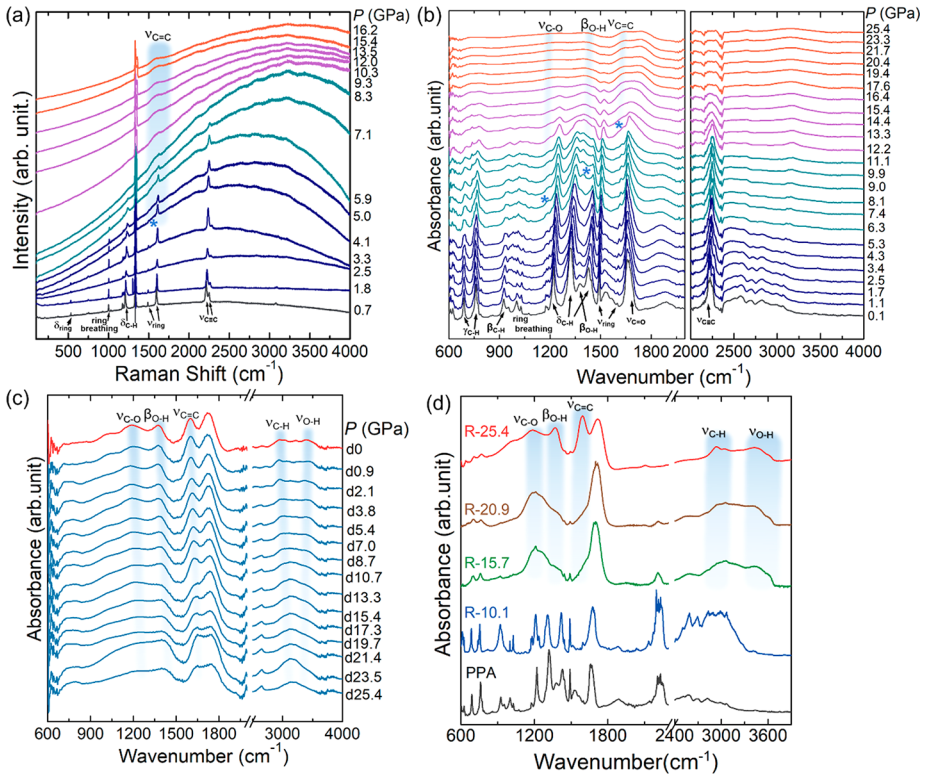

Figure 1. (a) In situ Raman spectra of PPA in the pressure range of 0.7−16.2 GPa upon compression. In situ IR spectra of PPA upon (b) compression and (c) decompression. (d) IR spectra of PPA and its polymerized product recovered from 10.1, 15.7, 20.9, and 25.4 GPa. The assignments of Raman and IR modes of PPA are shown in Table S1 and S2, respectively. δ, β, and ν represent the scissoring, the in-plane bending, and the stretching vibration, respectively.

https://doi.org/10.1021/acsapm.2c00728
ACS Appl. Polym. Mater. 2022, 4, 5246−5252

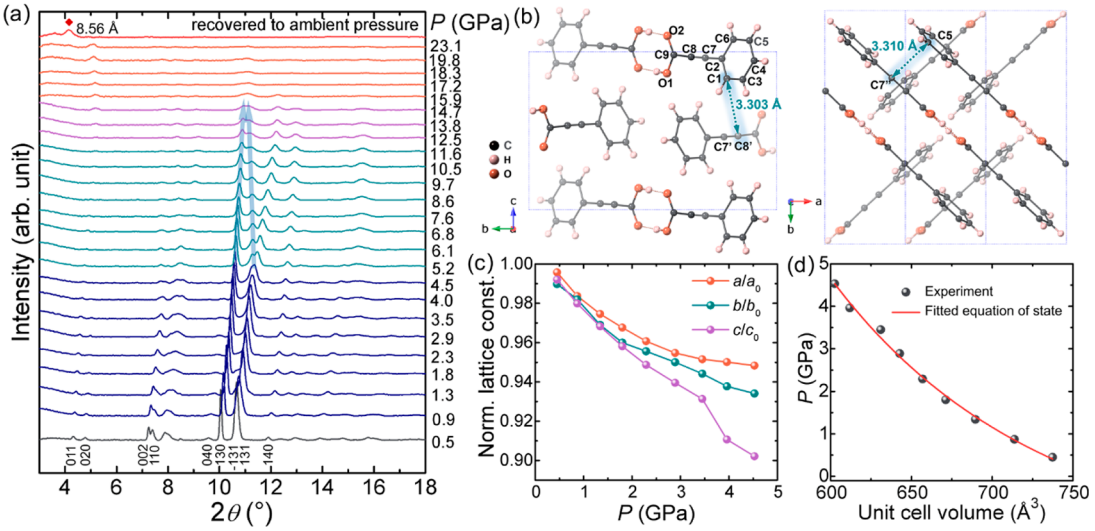

Figure 2. (a) Synchrotron XRD patterns of PPA under applied pressures. (b) Crystal structure of PPA at 4.5 GPa. The C···C distance along cross-stack and parallel-stack molecules, as demonstrated by the Rietveld refinement of XRD data. (c) Evolution of corresponding compression ratio of three axis from 0.5 to 4.5 GPa. (d) $P-V$ relationship of PPA fitting by the third-order Birch−Murnaghan equation of state.

Computation Details. The DFT calculations in this paper, including structural optimization and molecular dynamics simulation, were performed with the *Vienna Ab-initio Simulation Package* (*VASP*) code.[26] The local density approximation (LDA) exchange correlation functional by Ceperley and Alder, as parametrized by Perdew and Zunger (CA-PZ) was used with the projector-augmented plane-wave (PAW) potentials.[27] For structure optimization, a cutoff energy of 600 eV was set with k-point solution better than $2\pi \times 0.05$ A^{-1}, whereas molecular dynamics simulation was carried out with an energy cutoff at 560 eV and a Γ-point only sampling. First, the crystal structure of PPA at 4.5 GPa determined by refinement with XRD data was used to construct a supercell consisting of a $2a \times 2b \times 2c$ unit cell, and then the supercell was optimized at 10 GPa, followed by Hessian matrix calculation. At last, the simulations using metadynamic (MD)[28] method were worked out at 300 K. Each meta step takes 0.5 ps. NVT ensemble was used in MD simulation. DFT-D3(BJ)[29] correction was used to take the noncovalent effects into consideration.

AC Impedance Spectroscopy Measurement of PIP Product of PPA. The c-BN gasket for AC impedance spectroscopy measurement was prepared as described previously,[22] with the thickness of 45 μm and a hole of 240 μm. The PIP product of PPA was synthesized by symmetric DAC at 25 GPa. After sample loading, an external pressure of 0.6 GPa was applied to ensure the compaction. Thin platinum foils with a width of 300 μm were painted on both surfaces of the sample as electrodes. Silver glue and copper wires were used to connect the impedance spectrometer and the electrodes. The data were collected using the apparatus described in ref 22, with the AC voltage of 100 mV and frequency range of 0.1−32 M Hz. The data in the frequency range of 600−1 M Hz were fitted by Z-view to obtain the equivalent circuit diagram, resistance, and capacitance. The conductivity (σ) and permittivity (ε) were calculated by the formulas

$$\sigma = 1/RS \tag{2}$$

$$\varepsilon = Cl/S \tag{3}$$

Wherein l and S represent the thickness and cross-sectional area of the sample chamber, respectively.

RESULTS AND DISCUSSION

Polymerization of PPA under High Pressure. The evolution of the Raman spectra of PPA up to 16.2 GPa are shown in Figure 1a. As the pressure increases, all vibrational modes adopted blue shift, which is attributed to the reduction of interatomic distance. At 5.0 GPa, a new peak centered at ∼1547 cm^{-1} ascribed to the C═C stretching ($\nu_{C=C}$) appeared with the fluorescence enhanced dramatically, and the peaks from the phenyl (δ_{C-H} at 1245 cm^{-1}, ν_{ring} at 1615 cm^{-1}) and alkynyl ($\nu_{C\equiv C}$ at 2250 cm^{-1}) were significantly weakened and disappeared. The pressure dependence of Raman peaks is shown in Figure S1a, and chemical reaction can be clearly distinguished. The $\nu_{C=C}$ mode of poly-PPA was maintained during the decompression (Figure S1b), but cannot be clearly observed at recovered sample due to the high fluorescence background.

To avoid the influence of fluorescence, we also measured in situ IR spectra of PPA (Figure 1b, Figure S2a). Similar to the Raman spectra, the absorption peaks from the phenyl and alkynyl were weakened simultaneously and then disappeared gradually above 6.3 GPa, including the C−H stretching (ν_{C-H}), the C−H scissoring (δ_{C-H}) at 1240, 1350, and 1450 cm^{-1}, the ring stretching (ν_{ring}) at 1505 cm^{-1}, and the C≡C stretching ($\nu_{C\equiv C}$) at 2234 and 2290 cm^{-1}. New peaks appeared at ∼1185 cm^{-1} and ∼1400 cm^{-1} at 7.4 GPa, which are identified as single bonded C−O stretching (ν_{C-O}) and O−H in-plane bending (β_{O-H}) of the polymer. Subsequently, The C═C stretching ($\nu_{C=C}$, ∼ 1634 cm^{-1}) mode can be clearly distinguished at 12.2 GPa, and was enhanced with increasing pressure (Figure 1b, S2a). These series of transformations clearly demonstrated that phenyl and alkynyl reacted simultaneously to produce a polymer with sp^2−sp^3 carbon. When decompressed to ambient pressure (Figure 1c, Figure S2b), these modes still existed, and additional peaks at 3450 and 2935 cm^{-1} were also observed. These two bands are attributed to the O−H stretching (ν_{O-H}) and sp^3 C−H (ν_{C-H}) stretching in polymer, indicating new types of hydrogen bonds appeared. Further comparing the IR spectra of the samples recovered from different pressure (Figure 1d), we found that the C═C stretching was greatly enhanced with increasing pressure, demonstrating a higher polymerization degree in the sample R-25.4 (recovered from 25.4 GPa).

Structural Evolution under High Pressure. To analyze the PIP mechanism, we performed synchrotron XRD experiments in the pressure range of 0.5−23.1 GPa, and obtained the

https://doi.org/10.1021/acsapm.2c00728
ACS Appl. Polym. Mater. 2022, 4, 5246−5252

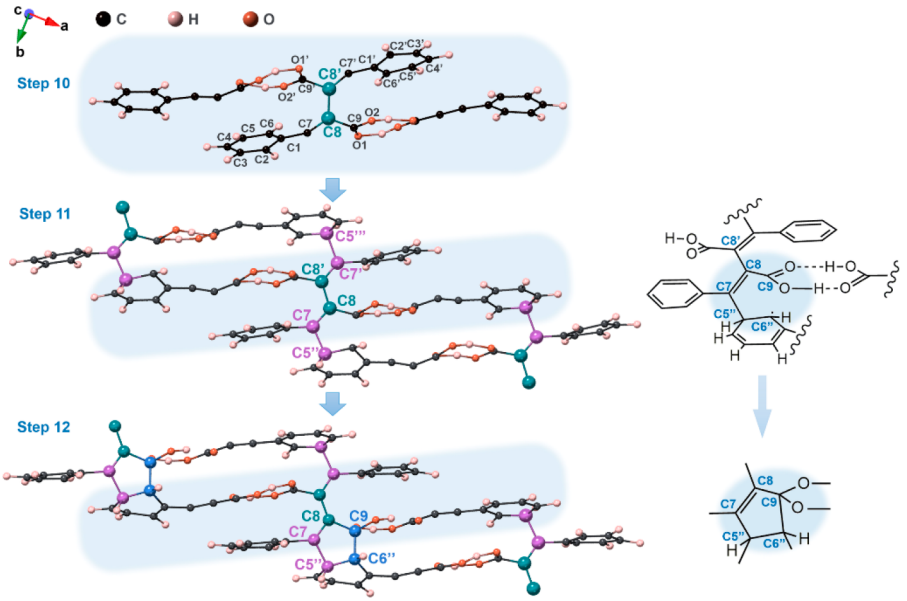

Figure 3. Crystal structure of PPA at 300 K and 10 GPa, simulated by metadynamics.

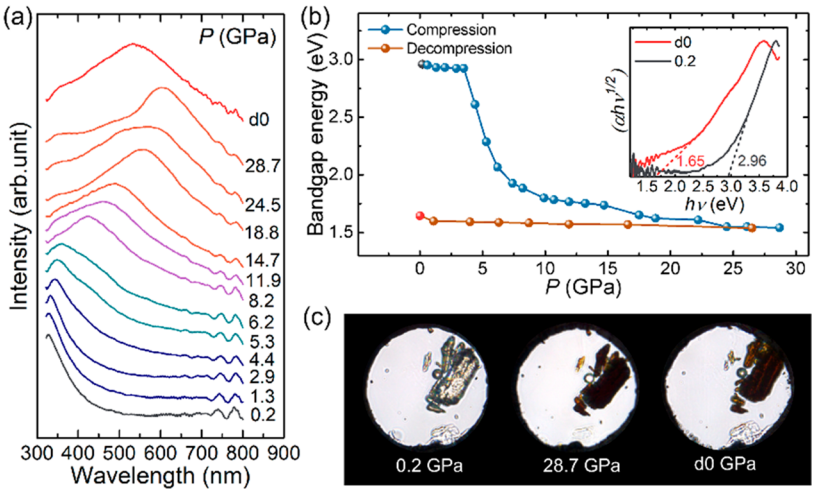

Figure 4. Optical characterizations of PPA under high pressure. (a) Selected UV−vis absorption spectra under high pressure. (b) Pressure-dependent values of bandgap energy. The inset in b shows the variations in $(\alpha h\nu)^{1/2}$ versus photon energy $h\nu$ of the PPA before compression and after decompression. (c) Optical micrographs of PPA crystals collected at selected pressures.

details of high-pressure structural evolution of PPA. The XRD peaks were marked using Miller indices, as shown in the Figure 2a. The XRD pattern of PPA at 0.5 GPa was well-fitted through Rietveld refinement (Figure S3a). It crystallized into a $P2_1/n$ space group, and the corresponding unit-cell parameters are a = 5.069(1) Å, b = 14.834(3) Å, c = 9.807(3) Å, α = 90°, β = 90.98(2)°, and γ = 90°. Apparently, there are two forms of molecular stacking, crossed and parallel, in its crystal structure (Figure S3b, S3c). With increasing pressure, all the XRD peaks of PPA moved to higher 2θ without generating new peaks. At 4.5 GPa, the diffraction peak observed at 11.3° (−1 3 1) is separated from 11.4° (1 3 1) and then merges with the 1 3 0 diffraction peak at 15.9 GPa (indicated by the arrow in Figure 2a), indicating anisotropic compression of the lattice. It is worth noting that they are almost along the lines connecting the centroids of alkyne groups and the centroids of phenyl groups in the next parallel molecules. Above 17.2 GPa and throughout the ensuing decompression process, most of the diffraction peaks disappeared and widened. There was only one obvious diffraction peak in the recovered polymer with a d value of 8.56 Å, which is close to the d-spacing of (0 1 1) of the reactant (Figure S4a). These indicate that the deteriorated crystallinity originating from disordered rearrangement of poly-PPA oligomers.

Because of the PIP of PPA, the original structure can only be fitted to 4.5 GPa (Figure 2b, Figure S4b). The compression ratio of three axis was obtained by performing the Rietveld refinement and shown in Figure 2c. The $P-V$ relationship of PPA was then fitted by the third-order Birch−Murnaghan (B-M) equation of state (Figure 2d):

$$P(V) = \frac{3}{2}B_0\left[\left(\frac{V_0}{V}\right)^{7/3} - \left(\frac{V_0}{V}\right)^{5/3}\right]\left\{1 + \frac{3}{4}(B_1 - 4)\left[\left(\frac{V_0}{V}\right)^{2/3} - 1\right]\right\} \quad (4)$$

https://doi.org/10.1021/acsapm.2c00728
ACS Appl. Polym. Mater. 2022, 4, 5246−5252

With V_0= 763 ± 10 Å^3, B_0 = 11 ± 2 GPa, and B_1 = 4.8 ± 1.3.

As shown in Figure 2b, the nearest C···C distances between adjacent cross-stack and parallel-stack PPA molecules at 4.5 GPa are $d_{C1\cdots C8'}$= 3.30 Å and $d_{C5\cdots C7''}$= 3.31 Å, respectively. This is similar to the critical PIP distance $d_{C\cdots C}$ = 3.3 Å reported for the phenyl-alkynyl synergistic reaction of TEB.[20]

An MD simulation was then performed to investigate the PIP process at 10 GPa and 300 K starting from a $2a \times 2b \times 2c$ supercell of this structure (Figure 3). The first reaction occurs at step 10 of the MD and is the bonding of alkyne carbon atoms C8−C8′ between adjacent molecules stacked in parallel packing mode. The closest C···C distance of PPA molecules, $d_{C5\cdots C7''}$, is then further shortened to bonding, demonstrating a synergetic reaction between alkynyl and phenyl groups. Hydrogen bond between carboxyl groups maintained the orderly stacking of oligomers and led to ordered chains. Therefore, the process hydrogen bond-assisted topochemical PIP of PPA has been demonstrated, and the product with a longer chain and a higher degree of π-conjugate backbone was confirmed. Further simulation shows that in step 12, the carbon atoms in phenyl and carboxyl groups undergo a complicated linkage to form a five-membered ring. This may be induced by the activation of the carboxyl carbon due to high pressure, which leads to the bonding of the C9 atom to the radical-bearing C6″ atom and the formation of a carbon ring. Meanwhile, the O atom attached to C9 atom is bonded to the neighboring H atom to form a new O−H bond, corresponding to the new ν_{O-H} mode (~3450 cm^{-1}) of the poly-PPA observed in the IR spectra. These processes can result in the expansion of the conjugate skeleton from a single molecule to multimolecules in the *ab* plane, thereby significantly affect the bandgap of the material.

In situ UV−vis absorption spectroscopy was utilized to measure the optical properties and bandgap evolution of PPA under high pressure (Figure 4a and Figure S5). At 0.2 GPa, the main absorption peak was around 327 nm with bandgap of 2.96 eV, which is designated as a $\pi \rightarrow \pi^*$ excitation of π electrons in the conjugated system consisting of phenyl and alkynyl. The carboxyl group acts with C≡C group as an auxochromic group. With further compression, the absorption spectra show distinct and continuous redshift to longer wavelengths (Figure S6). At 5.3 GPa, a new broad peak centered at 436 nm was observed representing the formation of PIP product. Especially, the absorption peak crosses over 300 nm in wavelength and finally covers the entire visible light region above 25 GPa. The bandgap energy was reduced to 1.54 eV at 28.7 GPa (Figure 4b). These properties suggested poly-PPA was a good candidate in optoelectronics. The extraordinary piezochromic transition of PPA is evidently seen through optical micrographs (Figure 4c). Upon compression, the crystals gradually darkened and eventually turned into opaque brown at 28.7 GPa. The transformation of absorption edge regulation (Figures S6 and S7) and piezochromism (Figure 4c, Figure S8) was completely irreversible, and the optical properties did not revert to the original state after decompression, corresponding to a bandgap value of 1.65 eV for the polymer (Figure 4b). This demonstrates the PIP of PPA greatly expanded the region of π-electron conjugation and the effective molecular chain length, forming a more $\pi-\pi$ conjugated system. With reference to the relationship between the number of double bonds and the absorption edge shift in polyene compounds,[30] a more than 10 conjugated π-electron system was speculated to be formed in the polymer. This is in good agreement with the product structures depicted in the MD simulations, also corresponding with the reaction observed in the Raman and IR spectra.

The π-conjugate structure in the poly-PPA significantly promoted the electrical conductivity. We conducted an AC impedance experiment on the PIP product synthesized at 25 GPa. An equivalent circuit was constructed to fit the semicircle in the Nyquist plot, as shown in the Figure 5. The permittivity

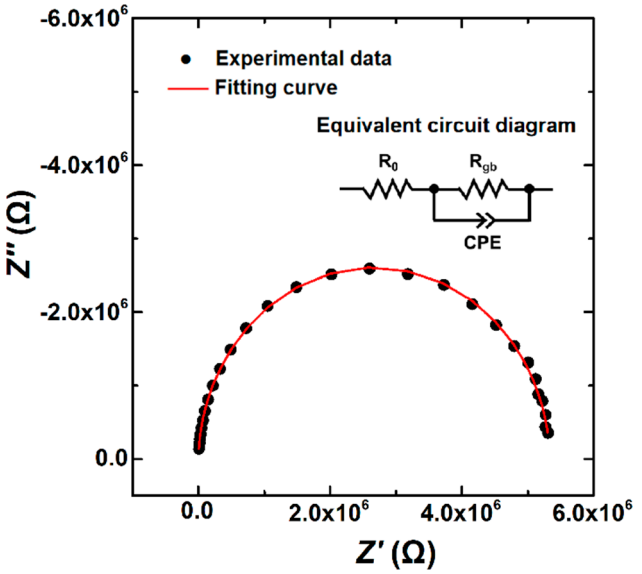

Figure 5. AC impedance spectrum of poly-PPA in the Nyquist plot. The equivalent circuit used for fitting is shown in the inset.

of the semicircle is ~3.0 × 10^{-11} F · cm^{-1}, which corresponds to the grain boundary.[31,32] This suggests that the grain boundary plays a major role in impeding electron migration. The corresponding conductivity is 1.24 × 10^{-6} S · cm^{-1}, which is greatly improved compared to the insulating reactant monomer. However, due to the existence of a large number of sp^{3}C and terminal groups of carboxyl, it is still significantly lower than that of the conductor (>1 × 10^2 S · cm^{-1}). The electron conductivity of the poly-PPA is similar to that of poly-DPB,[21] demonstrating the presence of a large $\pi-\pi$ conjugated system in its structure.

The synergetic reaction of PPA observed in this work differs significantly from that of DPB,[21] TEB,[20] and phenylacetylene.[11] There is a substantial synergistic impact on the alkyne and phenyl groups due to the initial step of polymerization between alkynyl groups, resulting in a significant reduction in reaction pressure. The critical C···C distance in this reaction is 3.3 Å, which is consistent with previous studies of DDA reactions, implying PIP depends on the distance between reactive carbon atoms. Despite the identity of C···C distance in two modes (Figure 2b), the bonding occurs only between parallel-stack PPA molecules, where the alkyne group is roughly aligned to the center of the phenyl group, and H-bonds are maintained on both sides. This also demonstrates that the crystal structure (including relative location and direction at threshold pressure, as well as intermolecular interactions) highly determines the direction of the topochemical reaction paths. Although hydrogen bonds can adhesion nearby molecules to some extent, the extensive and complicated bonding that happens in the *ab* plane makes it challenging to attain adequate crystallinity of the products. In

https://doi.org/10.1021/acsapm.2c00728
ACS Appl. Polym. Mater. 2022, 4, 5246−5252

the PIP reaction, stronger intermolecular interactions are expected to contribute to the reaction's orderliness and facilitate the large-scale high-pressure synthesis of the crystalline products.

CONCLUSION

In summary, we systematically investigated the structural evolution and polymerization mechanism of PPA under high pressure, and found that the alkynyl and phenyl groups undergo an arrangement-selective synergetic polymerization at 5 GPa, which is demonstrated by in situ Raman and IR spectroscopy. Combined with MD simulation, we verified the alkynyl-phenyl reactivity at much lower pressure than that in PIP of the reported aromatics, implying that the distance and stacking mode of unsaturated groups are the key factors of the pressure and reaction pathways of PIP. The carboxyl groups aid to maintaining a regular arrangement in the conjugate structure by forming intermolecular hydrogen interactions. Our study synthesized organic polymers with long π-conjugated backbone, lower bandgap energy and improved electrical conductivity via the PIP of PPA. This provides an inspiration for the goal-directed synthesis of organic photovoltaic materials by phenylethynyl compounds.

ASSOCIATED CONTENT

Supporting Information

The Supporting Information is available free of charge at https://pubs.acs.org/doi/10.1021/acsapm.2c00728.

Frequency shifts as a function of pressure ranging from 100 to 2350 cm^{-1}; in situ Raman spectra of PPA during decompression; in situ IR spectra of PPA upon compression and decompression; Rietveld refinement and crystal structure of PPA at 0.5 GPa; crystal structure and Rietveld refinement plot of PPA at 4.5 GPa; UV−vis absorption spectra of PPA during compression and decompression; pressure-dependent values of absorption edge; optical micrographs of PPA crystals; assignments of Raman and IR modes of PPA (PDF)

AUTHOR INFORMATION

Corresponding Author

Kuo Li − *Center for High Pressure Science and Technology Advanced Research, Beijing 100193, P. R. China;* orcid.org/0000-0002-4859-6099; Email: likuo@hpstar.ac.cn

Authors

Xuan Wang − *Center for High Pressure Science and Technology Advanced Research, Beijing 100193, P. R. China;* orcid.org/0000-0001-6647-9542

Xingyu Tang − *Center for High Pressure Science and Technology Advanced Research, Beijing 100193, P. R. China*

Xin yang − *Center for High Pressure Science and Technology Advanced Research, Beijing 100193, P. R. China*

Yida Wang − *Center for High Pressure Science and Technology Advanced Research, Beijing 100193, P. R. China*

Peijie Zhang − *Center for High Pressure Science and Technology Advanced Research, Beijing 100193, P. R. China;* orcid.org/0000-0001-6355-5482

Xiao Dong − *Nankai University, Key Laboratory of Weak-Light Nonlinear Photonics and School of Physics, Tianjin 300071, P. R. China*

Dongliang Yang − *Institute of High Energy Physics, Chinese Academy of Sciences, Beijing 100049, China*

Xujie Lü − *Center for High Pressure Science and Technology Advanced Research, Beijing 100193, P. R. China;* orcid.org/0000-0001-8402-7160

Haiyan Zheng − *Center for High Pressure Science and Technology Advanced Research, Beijing 100193, P. R. China;* orcid.org/0000-0002-4727-5912

Ho-kwang Mao − *Center for High Pressure Science and Technology Advanced Research, Beijing 100193, P. R. China*

Complete contact information is available at: https://pubs.acs.org/10.1021/acsapm.2c00728

Author Contributions

The manuscript was written through contributions of all authors. All authors have given approval to the final version of the manuscript.

Funding

National Natural Science Foundation of China (NSFC) (Grants 22022101, 21875006, 21771011, 21803033) National Key Research and Development Program of China (Grant 2019YFA0708502) Young Elite Scientists Sponsorship Program by Tianjin (Grant TJSQNTJ-2018−18)

Notes

The authors declare no competing financial interest.

ACKNOWLEDGMENTS

The authors acknowledge the support of the National Natural Science Foundation of China (NSFC) (Grants 22022101, 21875006, and 21771011). The authors also acknowledge the support of the National Key Research and Development Program of China (Grant 2019YFA0708502). X.D. thanks the support from NSFC (Grant 21803033) and Young Elite Scientists Sponsorship Program by Tianjin (Grant TJSQNTJ-2018-18). This work was carried out with the support of 4W2 beamline at Beijing Synchrotron Radiation Facility.

REFERENCES

(1) Yoo, C.-S. Chemistry under Extreme Conditions: Pressure Evolution of Chemical Bonding and Structure in Dense Solids. *Matter Radiat. Extrem.* **2020**, *5*, 018202.

(2) Yang, X.; Wang, X.; Wang, Y. D.; Li, K.; Zheng, H. From Molecules to Carbon Materials-High Pressure Induced Polymerization and Bonding Mechanisms of Unsaturated Compounds. *Crystals* **2019**, *9*, 490.

(3) Wang, X.; Li, K.; Zheng, H.; Zhang, P. Chemical Reactions of Molecules under High Pressure. *Chem. Bull.* **2019**, *82*, 387−398.

(4) Mao, H.-k.; Chen, B.; Chen, J.; Li, K.; Lin, J.-F.; Yang, W.; Zheng, H. Recent Advances in High-Pressure Science and Technology. *Matter Radiat. at Extremes* **2016**, *1*, 59−75.

(5) Chelazzi, D.; Ceppatelli, M.; Santoro, M.; Bini, R.; Schettino, V. Pressure-Induced Polymerization in Solid Ethylene. *J. Phys. Chem. B* **2005**, *109*, 21658−21663.

(6) Citroni, M.; Ceppatelli, M.; Bini, R.; Schettino, V. The High-Pressure Chemistry of Butadiene Crystal. *J. Chem. Phys.* **2003**, *118*, 1815.

(7) Trout, C. C.; Badding, J. V. Solid State Polymerization of Acetylene at High Pressure and Low Temperature. *J. Phys. Chem. A* **2000**, *104*, 8142−8145.

(8) Sun, J.; Dong, X.; Wang, Y.; Li, K.; Zheng, H.; Wang, L.; Cody, G. D.; Tulk, C. A.; Molaison, J. J.; Lin, X.; et al. Pressure-Induced Polymerization of Acetylene: Structure-Directed Stereoselectivity and a Possible Route to Graphane. *Angew. Chem., Int. Ed.* **2017**, *56*, 6553−6557.

(9) Ward, M. D.; Huang, H.-T.; Zhu, L.; Popov, D.; Strobel, T. A. High-Pressure Behavior of C_2I_2 and Polymerization to a Conductive Polymer. *J. Phys. Chem. C* **2019**, *123*, 11369−11377.
(10) Wilhelm, C.; Boyd, S. A.; Chawda, S.; Fowler, F. W.; Goroff, N. S.; Halada, G. P.; Grey, C. P.; Lauher, J. W.; Luo, L.; Martin, C. D.; Parise, J. B.; Tarabrella, C.; Webb, J. A. Pressure-Induced Polymerization of Diiodobutadiyne in Assembled Cocrystals. *J. Am. Chem. Soc.* **2008**, *130*, 4415−4420.
(11) Santoro, M.; Ciabini, L.; Bini, R.; Schettino, V. High-Pressure Polymerization of Phenylacetylene and of the Benzene and Acetylene Moieties. *J. Raman Spectrosc.* **2003**, *34*, 557−566.
(12) Li, X.; Baldini, M.; Wang, T.; Chen, B.; Xu, E.-S.; Vermilyea, B.; Crespi, V. H.; Hoffmann, R.; Molaison, J. J.; Tulk, C. A.; Guthrie, M.; Sinogeikin, S.; Badding, J. V. Mechanochemical Synthesis of Carbon Nanothread Single Crystals. *J. Am. Chem. Soc.* **2017**, *139*, 16343−16349.
(13) Ward, M. D.; Huang, H.-T.; Zhu, L.; Biswas, A.; Popov, D.; Badding, J. V.; Strobel, T. A. Chemistry through Cocrystals: Pressure-Induced Polymerization of $C_2H_2{\cdot}C_6H_6$ to an Extended Crystalline Hydrocarbon. *Phys. Chem. Chem. Phys.* **2018**, *20*, 7282−7294.
(14) Patyk, E.; Podsiadło, M.; Katrusiak, A. CH···N Bonds and Dynamics in Isostructural Pyrimidine Polymorphs. *Cryst. Growth Des.* **2015**, *15*, 4039−4044.
(15) Fanetti, S.; Santoro, M.; Alabarse, F.; Enrico, B.; Bini, R. Modulating the H-Bond Strength by Varying the Temperature for the High Pressure Synthesis of Nitrogen Rich Carbon Nanothreads. *Nanoscale* **2020**, *12*, 5233−5242.
(16) Nobrega, M. M.; Teixeira-Neto, E.; Cairns, A. B.; Temperini, M. L. A.; Bini, R. One-Dimensional Diamondoid Polyaniline-like Nanothreads from Compressed Crystal Aniline. *Chem. Sci.* **2018**, *9*, 254−260.
(17) Dunning, S. G.; Zhu, L.; Chen, B.; Chariton, S.; Prakapenka, V. B.; Somayazulu, M.; Strobel, T. A. Solid-State Pathway Control via Reaction-Directing Heteroatoms: Ordered Pyridazine Nanothreads through Selective Cycloaddition. *J. Am. Chem. Soc.* **2022**, *144*, 2073−2078.
(18) Huss, S.; Wu, S.; Chen, B.; Wang, T.; Gerthoffer, M. C.; Ryan, D. J.; Smith, S. E.; Crespi, V. H.; Badding, J. V.; Elacqua, E. Scalable Synthesis of Crystalline One-Dimensional Carbon Nanothreads through Modest-Pressure Polymerization of Furan. *ACS Nano* **2021**, *15*, 4134−4143.
(19) Wang, Y.; Dong, X.; Tang, X.; Zheng, H.; Li, K.; Lin, X.; Fang, L.; Sun, G.; Chen, X.; Xie, L.; et al. Pressure-Induced Diels-Alder Reactions in C_6H_6-C_6F_6 Cocrystal towards Graphane Structure. *Angew. Chem., Int. Ed.* **2019**, *5*, 1468−1473.
(20) Li, Y.; Tang, X.; Zhang, P.; Wang, Y.; Yang, X.; Wang, X.; Li, K.; Wang, Y.; Wu, N.; Tang, M.; Xiang, J.; Lin, X.; Lee, H. H.; Dong, X.; Zheng, H.; Mao, H.-k. Scalable High-Pressure Synthesis of sp^2-sp^3 Carbon Nanoribbon via [4 + 2] Polymerization of 1,3,5-Triethynylbenzene. *J. Phys. Chem. Lett.* **2021**, *12*, 7140−7145.
(21) Zhang, P.; Tang, X.; Wang, Y.; Wang, X.; Gao, D.; Li, Y.; Zheng, H.; Wang, Y.; Wang, X.; Fu, R.; Tang, M.; Ikeda, K.; Miao, P.; Hattori, T.; Sano-Furukawa, A.; Tulk, C. A.; Molaison, J. J.; Dong, X.; Li, K.; Ju, J.; Mao, H.-k. Distance-Selected Topochemical Dehydro-Diels-Alder Reaction of 1,4-Diphenylbutadiyne toward Crystalline Graphitic Nanoribbons. *J. Am. Chem. Soc.* **2020**, *142*, 17662−17669.
(22) Wang, X.; Tang, X.; Zhang, P.; Wang, Y.; Gao, D.; Liu, J.; Hui, K.; Wang, Y.; Dong, X.; Hattori, T.; Sano-Furukawa, A.; Ikeda, K.; Miao, P.; Lin, X.; Tang, M.; Zuo, Z.; Zheng, H.; Li, K.; Mao, H.-k. Crystalline Fully-Carboxylated Polyacetylene Obtained under High Pressure as a Li-ion Battery Anode Material. *J. Phys. Chem. Lett.* **2021**, *12*, 12055−12061.
(23) Mao, H. K.; Xu, J.; Bell, P. M. Calibration of the Ruby Pressure Gauge to 800 kbar under Quasi-Hydrostatic Conditions. *J. Geophys. Res.-Solid Earth.* **1986**, *91*, 4673−4676.
(24) Prescher, C.; Prakapenka, V. B. Dioptas: A Program for Reduction of Two-Dimensional X-ray Diffraction Data and Data Exploration. *High Pressure Res.* **2015**, *35*, 223−230.
(25) Petricek, V.; Dusek, M.; Palatinus, L. Crystallographic Computing System JANA2006: General Features. *Z. Kristallogr.* **2014**, *229*, 345−352.
(26) Kresse, G.; Furthmüller, J. Efficiency of Ab-Initio Total Energy Calculations for Metals and Semiconductors Using a Plane-Wave Basis Set. *Comput. Mater. Sci.* **1996**, *6*, 15−50.
(27) Perdew, J. P.; Zunger, A. Self-Interaction Correction to Density-Functional Approximations for Many-Electron Systems. *Phys. Rev. B* **1981**, *23*, 5048−5079.
(28) Barducci, A.; Bonomi, M.; Parrinello, M. Metadynamics. *Comput. Mol. Sci.* **2011**, *1*, 826−843.
(29) Grimme, S.; Ehrlich, S.; Goerigk, L. Effect of the Damping Function in Dispersion Corrected Density Functional Theory. *J. Comput. Chem.* **2011**, *32*, 1456−1465.
(30) Slepkov, A. D.; Hegmann, F. A.; Eisler, S.; Elliott, E.; Tykwinski, R. R. The Surprising Nonlinear Optical Properties of Conjugated Polyyne Oligomers. *J. Chem. Phys.* **2004**, *120*, 6807.
(31) Sinclair, D. C. Characterization of Electro-Materials Using AC Impedance Spectroscopy. *Bol. Soc. Esp. Cerám. Vidrio* **1995**, *34*, 55−65.
(32) Irvine, J. T. S.; Sinclair, D. C.; West, A. R. Electroceramics: Characterization by Impedance Spectroscopy. *Adv. Mater.* **1990**, *2*, 132−138.

Recommended by ACS

High-Pressure Synthesis of 1D Low-Bandgap Polymers Embedded in Diamond-like Carbon Nanothreads
Sebastiano Romi, Mario Santoro, *et al.*
FEBRUARY 16, 2022
CHEMISTRY OF MATERIALS
READ

Scalable High-Pressure Synthesis of sp^2–sp^3 Carbon Nanoribbon via [4 + 2] Polymerization of 1,3,5-Triethynylbenzene
Yapei Li, Ho-kwang Mao, *et al.*
JULY 23, 2021
THE JOURNAL OF PHYSICAL CHEMISTRY LETTERS
READ

Thermal Rearrangement Conversion of Cross-Linked *ortho*-Hydroxy Polyimide Networks
William Guzman, Jeffrey S. Wiggins, *et al.*
AUGUST 31, 2022
ACS APPLIED POLYMER MATERIALS
READ

Direct Synthesis of High-Melt-Strength Polypropylene Using the Fourth Generation Heterogeneous Ziegler–Natta Catalyst and Commercial Production...
Tsutomu Uzawa, T. C. Mike Chung, *et al.*
APRIL 13, 2020
ACS APPLIED POLYMER MATERIALS
READ

Get More Suggestions >

https://doi.org/10.1021/acsapm.2c00728
ACS Appl. Polym. Mater. 2022, 4, 5246−5252